A Physicomimetic Approach to Distributed Intelligence and Control of Autonomous Watercraft

Nikolaos I. Xiros[1(✉)] and Erdem Aktosun[2(✉)]

[1] Boysie Bollinger School of Naval Architecture and Marine Engineering, University of New Orleans, 2000 Lakeshore Dr, New Orleans, LA 70148, USA
nxiros@uno.edu

[2] Department of Shipbuilding and Ocean Engineering, İzmir Katip Çelebi University, Havaalanı Sosesi Cd, İzmir 35620, Turkey
erdem.aktosun@ikcu.edu.tr

Abstract. A square law of celestial mechanics is investigated as a driving virtual force law toward the development of swarms with distributes, i.e. not centralized, control and intelligence. It has been argued that decentralization of the control structure and task can enhance the robustness of the controllers involved and improve scalability. The approach in this work tackles the problem by adopting the concept of virtual forces which in this case follow the square law of attraction e.g. a nonlinear spring. The concept is adapted to the time and space, i.e. distance scales relevant to small, low-cost watercraft to be applicable. Various scenarios are investigated. All watercraft are assumed to have identical physical characteristics and dynamic responses but with small fluctuations and perturbations superimposed. Watercraft dynamics are simplified to model forward motion and rotation about the yaw axis; more detailed and precise models can also be used if desired or required. The local-loop controllers, which conventionally are called autopilots, ensure that the acceleration of the craft is adhering to the one dictated by the virtual, square law force field. Synthesis of the square law for the virtual force field involves amongst other feasibility of the derived governing dynamics as well as energy consumption, time to terminal conditions, etc.

1 Introduction

Unmanned Surface Vehicles (USVs) are self-contained unmanned untethered vessels that can transit on the surface of the water autonomously or through remote control. Unlike conventional manned surface vessels that are usually large and costly to build and operate, USVs are typically smaller in size and lower cost resulting from the reduced payload requirement due to being unmanned. In manned vessels, much of the volume and weight is necessary to support the activities (such as control, navigation, maintenance, and mission-related tasks), and sustainment (such as berthing, feeding, and entertainment) of the human occupants that recursively increases the size, vol-ume, and power requirements. USVs have no such requirements and therefore are typically many times smaller and more efficient than manned surface vessels.

D. Pavlou et al. (Eds.): OES 2023, SI 29, pp. 187–200, 2024.
https://doi.org/10.1007/978-3-031-49791-9_13

In the last two decades, significant effort has been invested in the development of Unmanned Underwater Vehicles (UUVs), while only a small effort has focused on Unmanned Surface Vessels/Autonomous Surface Vessels (USVs/ASVs). The major efforts in the design of USVs have focused on two areas: platforms for hydrographic data acquisition [1–3], and signal relay platforms that provide positioning and communications capabilities through the air-sea interface for UUVs [3–5].

The work presented here is part of a larger project that aims to develop a new concept for guidance and control of swarms of marine, or more general, vehicles based on a novel concept termed as robust probabilistic control. In particular, a low-cost solution to tackle the problem is currently under development that addresses the problem of navigation with minimal information exchange requirements.

(a) (b) (c)

Fig. 1. (a) The surface vehicle without most of her outfit (left) (b) unmanned underwater vehicle (middle) & (c) rotorcraft (right)

In this sense, a multi-purpose Autonomous Surface Vehicle (ASV) that is a low-cost mobile surface platform (Fig. 1a) has been designed and developed. The system is integrated with a motion measurement package to aid in navigation, and control, and to enhance dynamic performance. This single ASV can also be outfitted with acoustic communication systems to provide position updates and allow underwater vehicles, like in Fig. 1b, or agents to communicate while in transit and surveying. It is also possible to interact with the underwater vehicle to change the mission through an operator communicating with the USV via an RF uplink from shore or a distant vessel [6] or even a hovering aircraft like e.g. the extremely low-cost rotorcraft shown in Fig. 1c.

1.1 Potential Application Framework Formulation

The majority of tactical scenarios envisioned for performing autonomous underwater cueing for targets or objects (like proud mine-like objects, especially in large littoral areas), involve swarms (flotillas) of unmanned marine vehicles, underwater and possibly surface or even aerial. In specific, the proposed strategy for countermine operations relies on heterogeneous swarms in the sense that they consist of at least two types (tiers) of vehicles as shown in Fig. 2(a) A Tier-1 surface vehicle which can be a greater-scale version of the boat in Fig. 1a. This type of vehicle will carry radar, hull-mounted sonar,

compass, magnetometer(s) and proximity sensors, cameras (infrared or optical), GPS receiver(s), AIS and ECDIS as well as have the capacity to carry and deploy the platform of various sonar types which are unmanned underwater vehicles similar to the one in Fig. 1b or towed non-self-propelled platforms ("fish"). Further, the Tier-1 vehicles will carry considerable computing and communication assets necessary for the mission. (b) Tier-2 vehicles may be low-cost aerial units like the one shown in Fig. 1c outfitted with low-cost sensors like camera, GPS and compass as well as appropriate actuation for steering and throttle control.

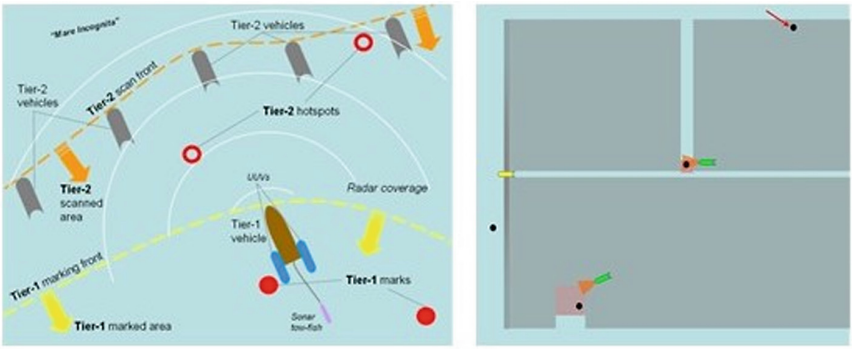

Fig. 2. An approach to mine detection and marking (a) 2-tier swarm structure, up and (b) 2D field of operations, down.

Various strategies have been proposed concerning the level of cooperation between the various vehicles as well as diversification of the flotilla in the sense of the number and types of vehicles used. However, up to now there is no general framework to comparatively assess these strategies and schemes. In this end, a unified performance index (or metric) is needed encompassing various quantities, reflecting mission accomplishment as well as the associated economic costs of system acquisition and operation.

Although, economic costs are more or less straightforward to define, mission accomplishment assessment needs in most cases some additional work. On the other hand, a generic performance index that comes to mind when military operations, financial or strategic decisions are of interest is probabilities associated with various events. Returning to the object cueing scenario and limiting our investigation here to a 2D rectangular area (or field) as shown in Fig. 2b, without significant loss of generality, the following spatial function (map) is introduced for any point (x,y) in our 2D area.

$f(x,y) = \mathbf{0}$ if target is ***not*** present at (x,y); **1** if target ***is*** present at (x,y).

Furthermore, we assume that f is time-invariant. Therefore, as time goes on any object cueing system covers an increasingly larger portion of the field and assigns 0 or 1 to each one of the points 'visited'; however, for each decision made there is an associated *probability of error* $p_e(x,y; t)$. It is noted here that the probability of error is time dependent because each point in the field may be 'revisited' as many times needed

and by any type of vehicles. Therefore, a reasonable setup of the object cueing problem is minimize t_0 for which it holds $p_e(x,y;\,t) < p_{e0}$ for $t > t_0$ and all (x,y) in the field.

If the economic costs of system acquisition and operation are included in the minimization problem above, then the overall problem can be approached by multi-objective optimization methods.

Solving the problem stated above requires the determination of various system parameters including but not limited to number of vehicles and vehicle types, vehicle speed, number of sensors and sensor types, level of cooperation, field coverage scheme etc. Evidently, additional constraints will be introduced to the problem due to the physics and engineering involved as e.g. vehicle speed ceiling, coverage scheme limitations due to maneuverability limitations etc.

A simple model for taking into account the main features of a possible configuration is shown in Fig. 2b. In this simplified version, there are two types of vehicles regardless of their implementation: Search vehicles (SV, shown in yellow) and Classification vehicles (CV, shown in green). Also, search sensors relying on the echoing principle (e.g. sonar) are considered.

SVs are equipped with non-classifying, long-range, side-scanning sensors. They provide with field scans of resolution decreasing with respect to the distance from the vehicle. As shown in Fig. 2b, the area marked as a result of an echo signal is increasing with the round trip time of the signal. Furthermore, this area is in any case larger than the area covered by the target itself as there are a number of uncertainties involved, including the positioning uncertainty of the SV. By assuming a 'line-of-sight' (LOS) mode of operation for the sensors, any target detected causes obstruction of view; therefore, the area 'behind' a detected target cannot be scanned unless the SV approaches the obstructed area from another angle or during another pass.

The probability of error for any point *inside the region scanned* by a specific SV, v, up to time t is given by the following relationship.

$$\begin{aligned} p_e(x,\,y;\,\mathrm{v@t}) = {} & f(x,\,y)\,\mathrm{x}\,p_{miss}(\boldsymbol{d} < (x,\,y),\,\mathrm{trajv@t>}) \\ & + [1 - \mathrm{f}(x,\,y)]\,\mathrm{x}\sum\{[1 - p_{miss}(\boldsymbol{d} < (x_k,\,y_k),\,\mathrm{traj\{v;t\}>})] \\ & \mathrm{x}\,p_{1|0}(x,\,y;\,x_k,\,y_k;\,\mathrm{traj\{v@t\}})\} \end{aligned}$$

In the above, $\boldsymbol{d} < (x,y),\mathrm{traj\{v@t\}} >$ stands for the Euclidean distance of a point (x,y) from the trajectory, traj{v@t}, of the specific SV, v, up to time t; if not defined is set to infinity.

Distribution $p_{\mathrm{miss}}(\boldsymbol{d} < (x,y),\mathrm{traj\{v@t\}} >)$ refers to the probability density function to *miss* a target in the manner indicated by the red arrow in Fig. 2, provided that point (x,y) lies in the area encompassed by a target; $p_{\mathrm{miss}}(\boldsymbol{d} < (x,y),\mathrm{traj\{v@t\}} >)$ is expected to be an increasing function of $\boldsymbol{d} < (x,y),\mathrm{traj\{v@t\}} >$ and actually to saturate to unity if this distance lies above a threshold. Also, p_{miss} depends on the capabilities of the sensors mounted on the SV.

Distribution $p_{1|0}$ stands for the probability density function that a point (x,y) belongs to the marking area assigned to the k-th target, if detected by SV v until time t. It is reasonable to assume that $p_{1|0}$ is a decreasing function of the distance of point (x,y) from the center location of the k-th target (the larger the distance between the two points the

less probable to be included in the same 'patch') and an increasing function of $\boldsymbol{d} <$ (x_k,y_k),traj{v;t} > because of the 'spreading' caused by reduced sensor resolution in the far field.

$$p1|0(x, y; x_k, y_k; \text{traj v@t}) = p1|0(\boldsymbol{d} < (x, y), (x_k, y_k) >, \boldsymbol{d} < (x_k, y_k), \text{traj v;t} >)$$

In the above, $\boldsymbol{d} <$ (x_1,y_1),(x_2,y_2) > stands for the Euclidean distance between two points on the plane.

It would be the summation in the relationship for $p_e(x,y;$ v@t) spans all the targets in the field of interest. If (x,y) does not lie in the region already scanned by the specific SV, v, until time t, it is easy to verify that $p_e(x,y;$ v@t) = 1 if f(x,y) = 1 and $p_e(x,y;$ v@t) = 0 if f(x,y) = 0 and no target in some vicinity of (x,y) has been scanned yet. Although, it could have been defined differently, these facts make intuitive sense.

The relationship for $p_e(x,y;$ v@t) is valid provided some underlying assumptions hold. The targets must be distributed *reasonably sparse* so that the patches marked for two or more neighboring objects by the SVs do not overlap. Furthermore, the probability of 'spontaneous triggering' of the sensors, in the sense that they detect a target at a point where none is present in the vicinity, is considered negligible. Although these assumptions simplify the expression for $p_e(x,y;$ v@t), they can be dropped, if needed, by appropriate extensions.

A way to tackle such requirements expressed in a probabilistic framework is to consider techniques *Robust Stochastic Control.* Indeed, stochastic control deals with systems where the objective is to minimize or maximize the probability of an event related to a dynamic system or random signal by manipulating one or more of a driving signal. In conventional stochastic control, e.g. [7–9], the full dynamics of the process or system under control is considered. Given recent advances in self-organization, however, an alternative path could be followed. Specifically, the swarm's vehicles will be driven by local, decentralized and in effect distributed deterministic control laws that require the knowledge by each vehicle of its own motion or other variables as well as those of the immediately neighboring units, but in no case the state variables of the entire formation. This scheme is usually implemented as a set of "virtual forces" exerted between neighboring vehicles, resembling the forces arising between the molecules or particles of a solid, liquid or gaseous substance; thereof the term physicomimetics or artificial physics. A critical step needed towards the direction of applying this technique, which is referred to as Robust Probabilistic Control is the migration from the concept of trajectories employed to describe the time evolution of the phase (state) space of a dynamical system to that of the *phase space probability distribution function* (or *measure*), $\rho(q,p;t)$ of the dynamical system. Consider a dynamical system with canonical coordinates q_i and conjugate momenta p_i, where $i = 1,\ldots,n$. Then the phase space distribution $\rho(q,p)$ determines the probability $\rho(q,p)d^nqd^np$ that the system will be found in the infinitesimal phase space volume d^nqd^np. The concept and its applications will be investigated in full detail in a follow-up work.

Probabilistic measures of mission success like the ones introduced earlier can in turn be linked to individual vehicle dynamics through Liouville's Theorem. This theoretical tool depicts the dynamics of the collective behavior of an autonomous swarm on the basis of the phase-space probability distribution measure concept, instead of some more conventional approach based on individual vehicle trajectories. Specifically, Liouville's theorem governs the evolution of the distribution function $\rho(q,p;t)$ in time according to the following partial differential equation:

$$\frac{d\rho}{dt} = \frac{\partial \rho}{\partial t} + \sum_{i=1}^{n}\left(\frac{\partial \rho}{\partial q_i}\dot{q}_i + \frac{\partial \rho}{\partial p_i}\dot{p}_i\right) = 0 \tag{1}$$

As a direct consequence of Liouville's theorem, the following equation can be obtained for the distribution function of a swarm's phase space.

$$\frac{\partial \rho}{\partial t} = [H, \rho] \tag{2}$$

where H is the Hamiltonian and the Poisson bracket between two functions of the canonical coordinates is defined by the following.

$$\left[f, g\right] = \sum_{i=1}^{n}\left(\frac{\partial f}{\partial q_i}\cdot\frac{\partial g}{\partial p_i} - \frac{\partial f}{\partial p_i}\cdot\frac{\partial g}{\partial q_i}\right) \tag{3}$$

The Newtonian equation of motion for each swarm vehicle will, in effect, assume the following form.

$$\vec{\mathbf{a}}_i = \frac{1}{m_{\mathrm{i,virtual}}}\cdot \sum_{\substack{j \\ i \neq j}} \vec{\mathbf{F}}_{\mathrm{ij,virtual}} \tag{4}$$

In the above, $\mathbf{a}_i$ is the acceleration of the i-th vehicle, $m_{i,\mathrm{virtual}}$ the virtual mass assigned to the vehicle by the artificial physics, and $\mathbf{F}_{ij,\mathrm{virtual}}$ the virtual force exerted on the i-th vehicle by the j-th neighbor per the physicomimetic interaction law governing the swarm dynamics.

The challenges related with swarm vehicle navigation and guidance are complex and can only be tackled using a comprehensive and non-trivial framework for the design of the local-loop controller that can guarantee compliance of the vehicle to artificial physics dynamics. The actual equation of motion of an arbitrary vehicle, assuming a material point model, is as follows.

$$\vec{\mathbf{a}}_i = \frac{1}{m_i}\cdot\left[\sum \vec{\mathbf{F}}_{\mathrm{exogenous}} + \sum \vec{\mathbf{F}}_{\mathrm{control}}\right] \tag{5}$$

In the above, m_i is the actual mass of the i-th vehicle, $\mathbf{\Sigma F}_{\mathrm{exogenous}}$ the resultant exogenous force exerted on the i-th vehicle by the environment and $\mathbf{\Sigma F}_{\mathrm{control}}$ the resultant control force exerted on the i-th vehicle by thrusters, control surfaces etc. To make vehicle

dynamics comply to artificial physics, as defined in the previous task, the resultant control force has to be as follows.

$$\sum \vec{\mathbf{F}}_{\text{control}} = \frac{m_i}{m_{\text{i,virtual}}} \cdot \sum_{\substack{j \\ i \neq j}} \vec{\mathbf{F}}_{\text{ij,virtual}} - \sum \vec{\mathbf{F}}_{\text{exogenous}} \tag{6}$$

The above clearly shows the issues that may arise if the physicomimetic control law generates excessively high forces or the virtual mass value is small compared to the actual mass value of the vehicle. This can lead to excessive control force requirements that can make the artificial physics scheme infeasible. This is why the local-loop controller design is a non-trivial aspect and needs to be investigated at least for one type or class of practical vehicles.

As in other similar cases, two or more subsystems either linear or nonlinear and either lumped or distributed, are coupled through processes that commonly are highly nonlinear. In our case, an appropriate identification method is employed, as explained later on, which comes as a generalization of the identification methodology for linear systems in phase-plane. Since the physicomimetic governing control laws may need to be continuously reconfigured, the option to adapt accordingly the gains of the local-loop controllers will be investigated in order to implement them in a follow-up effort. Such an approach will further increase system responsiveness and adaptability. Such adaptability enables for broad real-time reconfiguration of an autonomous swarm which in turn could convert routinely multi-sortie missions, due to the need for off-line reconfiguration, to single-sortie ones not needing real-time oversight. The above work clearly demonstrates the need for vehicle dynamics identification for local-loop controller tuning and adaptation which will be addressed in future work.

2 Methodology

The methodology is now investigated in the case of a single vehicle. The physicomimetic control law is that of a nonlinear spring with a quadratic force law. One end of the virtual spring is attached to the origin which is the homing point the vehicle needs to reach. The free end of the spring is attached to the center of mass of the vehicle. A second rotational nonlinear spring-like mechanism applies to adjusting the heading of the vehicle, so that the centerline (longitudinal stern-bow) axis of the vehicle boat gets aligned with that of the onboard radius vector pointing from the vehicle's center to the origin (target).

Figure 3 shows the supervisory controller with a discrete-time model. We use this model to implement the control law with the feedback information. As can be seen, the supervisory controller generates forward speed and yaw rate setpoints. The feedback controller then, if designed properly, makes sure that the setpoints issued by the supervisory controller are implemented and followed. This is achieved by using the thrusters and maneuvering assets of the boat. We now focus on the algorithm generating the setpoints, while in a future work the feedback controller synthesis will be addressed too.

In particular, consider the setup shown in Fig. 4, the vehicle (boat) is shown on a plane map at a certain location determined by the x-and y-coordinate (North-South and

East-West axis respectively). The vehicle is assumed to have (significant) speed along its centerline axis only pointing forward. The heading of the vehicle i.e. the angle of its forward velocity with respect to the North semiaxis is the third and final degree of freedom considered. As a result, the feedback information to implement the control law is the x-and y-coordinate as well as the compass reading for heading angle ψ. Using these, the onboard radius r and its angle with respect to the semiaxis pointing to the North can be calculated as the angle ϕ in the range $-\pi \leq \varphi < \pi$, calculated as follows.

$$r = \sqrt{x^2 + y^2}, \cos\varphi = \frac{x}{r}, \sin\varphi = \frac{y}{r} \tag{7}$$

Also, in this plane setup, the coordinates of the vehicle's velocity vector can be calculated as follows, where υ is the velocity (magnitude) of the vehicle.

$$v_x = v\cos\psi, v_y = v\sin\psi \tag{8}$$

In effect, the following approximate numerical integration equations over time can be used to simulate the vehicle kinematics:

$$x(t + \Delta t) = x(t) + v_x(t)\Delta t \tag{9}$$

$$y(t + \Delta t) = y(t) + v_y(t)\Delta t \tag{10}$$

$$\psi(t + \Delta t) = \psi(t) + \omega(t)\Delta t \tag{11}$$

In the above, t is time and Δt an appropriately small integration time step; omega (ω) stands for the rotational speed of the vehicle about an axis perpendicular to the xy-plane and with origin at the center of the vehicle.

Based on this framework, angle θ between the onboard radius vector pointing from the vehicle to the origin (target) and the vehicle's velocity vector can be calculated as follows (see Fig. 4).

$$\theta = \left(\frac{\pi}{2} - \varphi\right) + \frac{\pi}{2} + \psi = \psi - \varphi + \pi \tag{12}$$

Then a control law for a Supervisory Vehicle Controller, issuing forward speed and heading velocity setpoints, υ_{set} and ω_{set} correspondingly can be introduced as follows.

$$v_{set} = \begin{cases} g(\theta)\left(\frac{r}{R}\right)^2 v_{max}, 0 \leq r < R \\ g(\theta)v_{max}, r \geq R > 0 \end{cases}, \omega_{set} = \frac{\omega_{max}}{2} f(\theta) \tag{13}$$

$$g(\theta) = 1 - \frac{|\theta|}{\pi}, f(\theta) = \mathrm{sgn}(\theta)(\cos\theta - 1), \mathrm{sgn}(\theta) = \begin{cases} +1, \theta > 0 \\ 0, \theta = 0 \\ -1, \theta < 0 \end{cases} \tag{14}$$

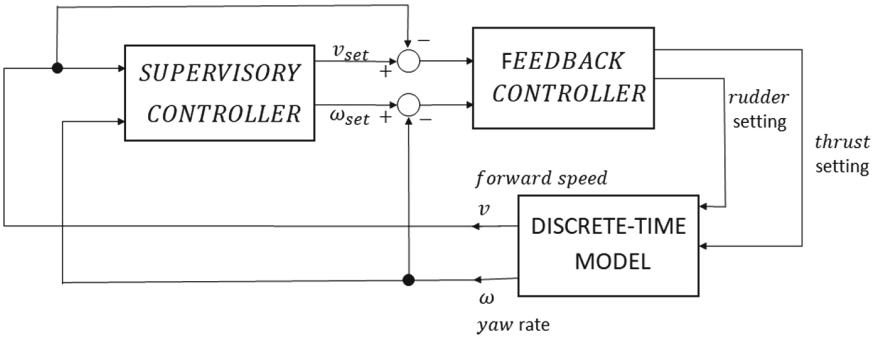

Fig. 3. Supervisory controller with discrete-time model

It is easy to see that $0 < v_{set} \leq v_{max}$ and $-\omega_{max} \leq \omega_{set} \leq \omega_{max}$; values $\upsilon_{\max}$ and $\omega_{\max}$ represent the maximum forward and rotational speed values that the vehicle can attain. Distance value R is a user-defined range; this can be defined as e.g. twenty times the vehicle's length and in any case, it is sufficiently large so the vehicle can attain its maximum forward speed without the risk of overshooting the target.

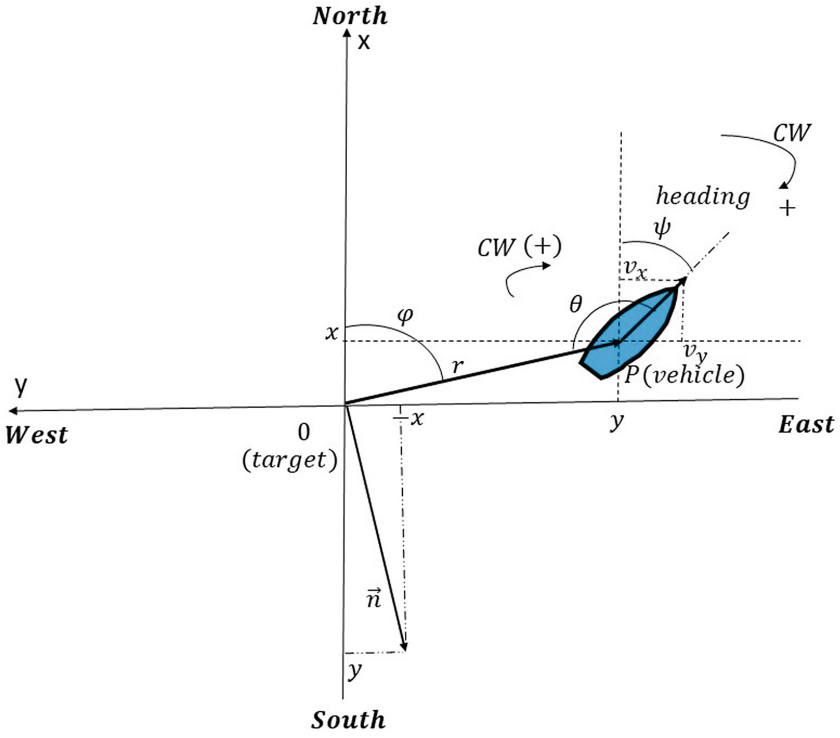

Fig. 4. Geometry of vehicle kinematics with the target point at the origin.

Since the control law is nonlinear, its performance can only be assessed through simulation, asymptotic analysis and qualitative arguments. Simulation results will be presented in the next section. For asymptotic analysis the following facts are noted.

If $\theta \approx \pm\pi$, then

$$v_{set} \approx 0, \omega_{set} \approx -\omega_{max}\text{sgn}(\theta) \tag{15}$$

If $\theta \approx \pm\pi/2$, then

$$v_{set} \approx \begin{cases} \left(\frac{r}{R}\right)^2 \frac{v_{max}}{2}, 0 \leq r < R \\ \frac{v_{max}}{2}, r \geq R \end{cases}, \omega_{set} \approx -\frac{\omega_{max}}{2}\text{sgn}(\theta) \tag{16}$$

If $\theta \approx \pm 0$, then

$$v_{set} \approx \begin{cases} \left(\frac{r}{R}\right)^2 v_{max}, 0 \leq r < R \\ v_{max}, r \geq R \end{cases}, \omega_{set} \approx \left(-\frac{\omega_{max}}{4}\right)|\theta|\theta \tag{17}$$

Given these observations, and assuming vehicle is initially at some arbitrary point and with arbitrary heading, it is first attempted to align the centerline axis with the onboard radius. Only then the vehicle is allowed to attain forward speed depending upon its distance from the target and relative to range R. As the vehicle gets closer to the target, forward speed decreases quadratically with distance, and corrections are applied so that the centerline remains aligned to the onboard radius.

3 Results and Discussion

The simulations based on physicomimetic control law were conducted in an attempt to model the behavior of a swarm of boats, using a methodology that had previously only been discussed with a single boat. To conduct the simulations, a total of 60 boats were selected, and the simulations themselves ran for a duration of 10 min. To begin the simulations, a set of initial conditions were established. These included the distance of each boat from its starting point, as well as the initial angles of both the φ and the heading angles of each boat. In addition, all boats were initially at rest, meaning that they had no forward speed at the beginning of the simulation. Throughout the course of the 10-min simulation, the movements and interactions of the boats with one another were tracked and analyzed. This allowed researchers to gain insights into how a swarm of boats might behave in a real-world scenario, and to identify any patterns or trends that could be useful in developing new strategies for navigating and controlling large groups of vessels.

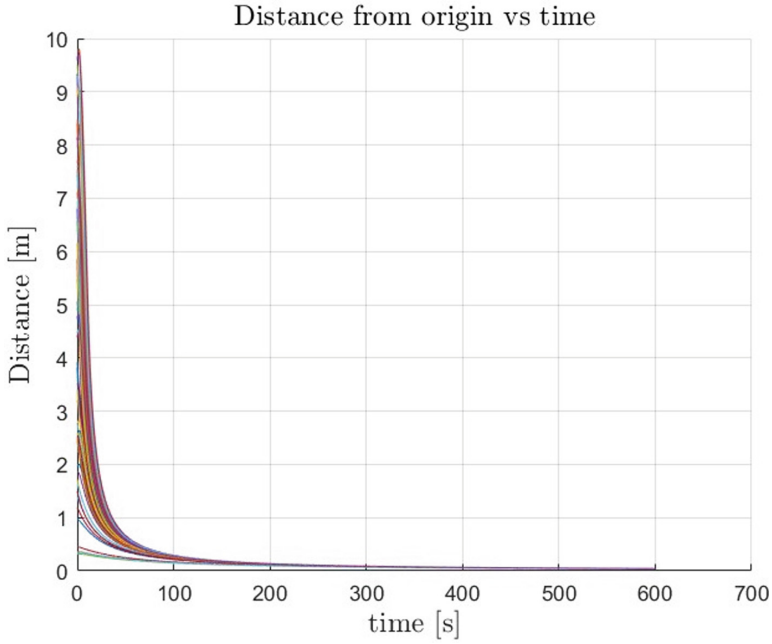

Fig. 5. Distance from origin with time for the boats' swarm

In Fig. 5, we can observe the distance that each of the 60 boats covered from their starting positions to their intended target. The initial conditions for the boats were chosen randomly. As evident from the figure, all 60 boats were able to reach the same target within a simulation period of 10 min.

Figure 6 displays the phase portraits of a group of boats acting as a swarm, with the θ angle as the primary axis. The figure shows the starting positions of the boats, which are determined by their distance from each other and the angle formed by that distance and their heading. The plot reveals that the phase portraits are spread out across a wide area, indicating a significant amount of dispersion among the boats.

Figure 7 is a visual representation of selected samples from the simulations, showcasing individual plots of six out of the total 60 samples. These individual plots provide a detailed depiction of the boat's movement during the simulation, including its forward speed and yaw rate, as well as important angles and trajectory. The plot effectively illustrates how each boat moves through the simulation, making it a valuable tool for analysis and understanding of the simulation results.

The results of our analysis indicate that when multiple boats are present, their trajectories do not intersect. This means that even though the boats may approach each other, they never cross paths and collide with one another. For example, when we examine a particular trajectory of a boat in the diagram, we can see that it converges smoothly with the trajectories of other boats without any collision occurring. To provide more information about the movement of boats, we can consider how a boat moves toward its destination. Initially, the boat starts from an arbitrary location and follows a curvy

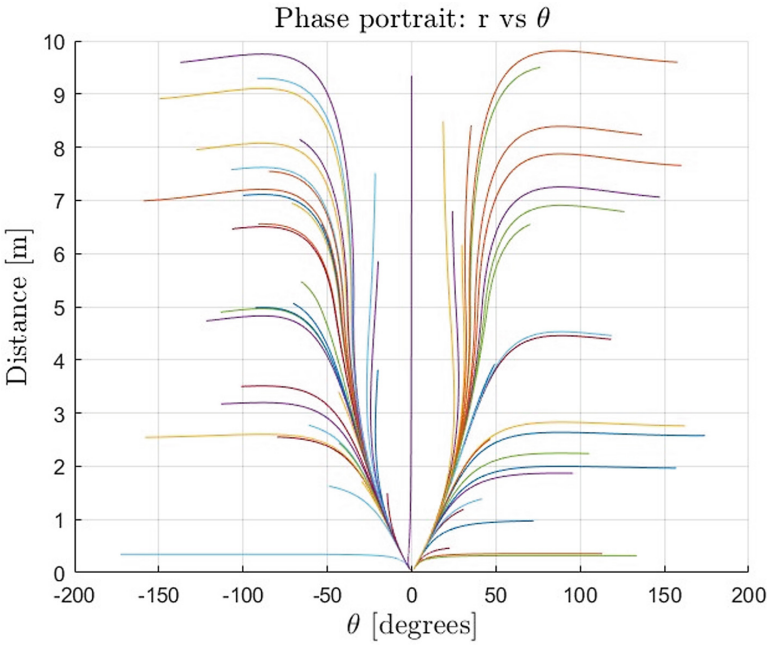

Fig. 6. Phase portraits of boats' swarm

path to reach its target. Our simulations reveal that the boat can move faster if it is fully aligned with and pointing toward the origin. This alignment ensures that the boat moves directly toward its intended target and does not waste energy moving away from it. On the other hand, if the boat is pointing away from the origin, it cannot move forward as efficiently because it has to use energy to move away from its intended target before it can start making progress toward it. As a result, the boat's progress is slower, and it may take longer to reach its destination.

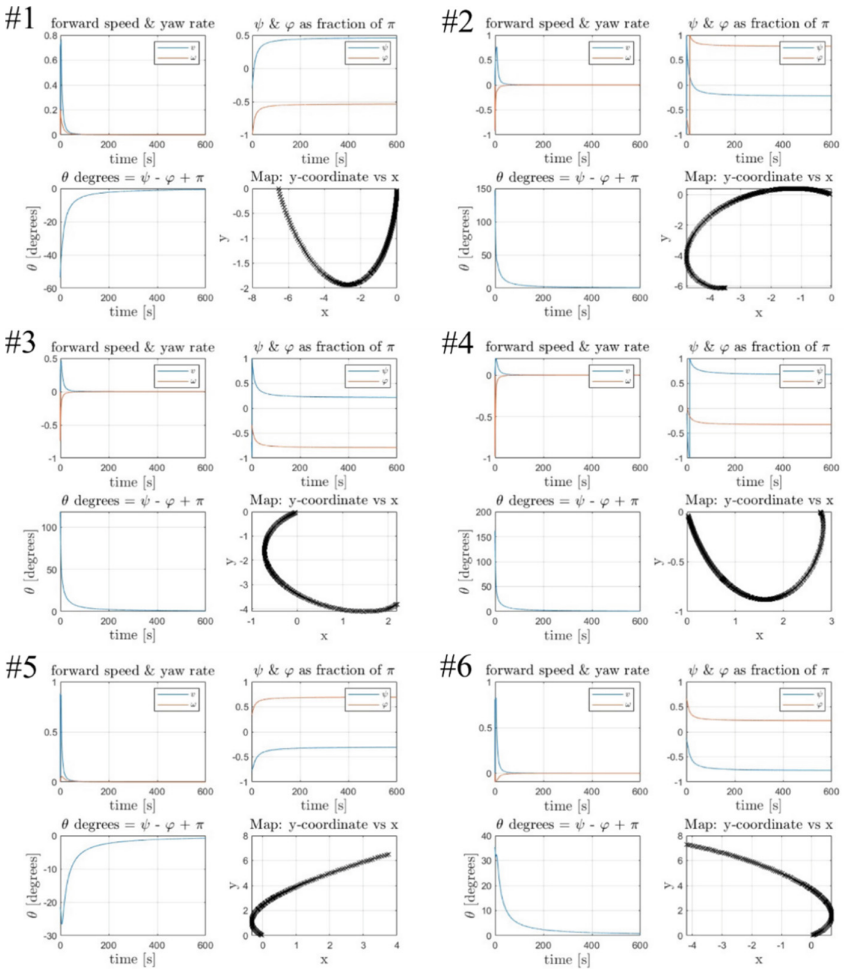

Fig. 7. 6 samples cases among all 60 cases

4 Conclusion

The present work presents research related to homing of an autonomous watercraft swarm using a distributed control law. A swarm of 60 boats is investigated in a simulation. Each vehicle is outfitted with a physicomimetic control law. The boats are assumed to have the same physical characteristics and responses, and their tracks are simplified to only consider motion and rotation around the yaw axis. The simulation investigates how the swarm of boats can be more energy-efficient through autonomous control. In future studies, the focus may shift to tuning local controllers and identifying boat dynamics in greater detail.

References

1. Chaumet-Lagrange M, Loeb H, Ygorra S. Design of an autonomous surface vehicle (ASV). In: Proceedings of OCEANS'94. 1994. p. I–120.
2. Manley JE. Development of the autonomous surface craft" aces". In: Oceans' 97 MTS/IEEE Conference Proceedings. 1997. p. 827–32.
3. DSOR. CARAVELA Development of a Long-Range Autonomous Oceanographic Vessel in Dynamic Systems and Ocean Robotics lab [Internet]. 1998. Available from: https://welcome.isr.tecnico.ulisboa.pt/projects_cat/dsor/
4. Oliveira P, Pascoal A, Rufino M, Sebastião L, Silvestre C. The DELFIM Autonomous Surface Craft. Rep (December 1999). 1999;
5. Oliveira P, Pascoal A, Kaminer I. A nonlinear vision based tracking system for coordinated control of marine vehicles. IFAC Proc Vol. 2002;35(1):295–300.
6. Leonessa A, Beaujean P-P, Driscoll F. Development of a small, multi-purpose, autonomous surface vessel. 2003.
7. Xiros NI, Logis E, Gasparis E, Tsolakidis S, Kardasis K. Theoretical and experimental investigation of unmanned boat electric propulsion system with PMDC motor and waterjet. J Mar Eng & Technol. 2009;8(2):27–43.
8. Xiros NI, Logis E, Charitos G. An automatic steering system for robust disturbance rejection. IASME Trans. 2004;1(2).
9. Fossen TI. Guidance and control of ocean vehicles. Univ Trondheim, Norway, Print by John Wiley & Sons, Chichester, England, ISBN 0 471 94113 1, Dr Thesis. 1999;